Supplements

Article title: **The more the better? A limited proportion of deep roots maximises tree survival under drought in Mediterranean forest**

Authors: Lucas Mondon, Nicolas Martin-StPaul, Gregor Rickert, Isabelle Maréchaux, Arsène Druel, Quentin Chaffaut, Damien Jougnot, Nicolas Delpierre, Marc Pessel, Ilhan Özgen-Xian, Hervé Cochard, Simon D. Carrière

The following Supporting Information is available for this article:

Section S1. Methods

Water from xylem samples was extracted by cryogenic vacuum distillation (Ehleringer and Osmond 1989; West et al. 2006). The stems were quickly cut into small pieces and placed in a flask heated to 90 to 100 °C for 1 hour. The water was collected in two successive liquid nitrogen traps. Generally, 3 to 5 ml of xylem water was extracted. These liquid samples were stored in small vials until analyzed.

Precipitation and deep water samples were analyzed on a Los Gatos Isotope Ratio Infrared Spectrometer (IRIS) at the University of Avignon (LGR DLT-100 liquid water stable analyzer accuracy ±0.2‰ vs V-SMOW for $\delta^{18}O$). However, because of possible spectral perturbations of IRIS measurements due to organic contaminants in xylem and drainage samples (Martín-Gómez et al. 2015), $\delta^{18}O$ of xylem and drainage samples were also analyzed using the Isoprime Isotope Ratio Mass Spectrometer (IRMS) at the LAMA laboratory of HydroSciences Montpellier, using the CO_2 equilibration technique in dual inlet mode, yielding $\delta^{18}O$ results with a ±0.6‰ precision. The isotopic ratios in this study are expressed as:

$$\delta^{18}O = \left[\left(\frac{R_{sample}}{R_{standard}}\right) - 1\right] \times 1000\ ‰ \qquad \text{(S1)}$$

Where R_{sample} and $R_{standard}$ are the heavy/light isotope ratios ($^{18}O/^{16}O$) of the sample and the standard (Vienna Standard Mean Ocean Water (VSMOW)), respectively.

Table S1. *Descriptions, origins and implemented values of all species-dependent parameters*

Parameter	Unit	Description	Model sensitivity*	Source of the value	Implemented values		
					Q.i	*F.s*	*A.a*
P50_VC_Stem	MPa	Water potential causing 50% of loss of hydraulic conductance in stem	High	Literature and direct measurements	-7[a]	-3.25[b]	-3.5[c]
slope_VC_Stem	$\%.MPa^{-1}$	Slope of rate of leaf embolism spread at $P50_{Stem}$	Low	Literature and direct measurements	30[a]	71[b]	135[c]
P50_VC_Leaf	MPa	Water potential causing 50% of loss of hydraulic conductance in leaf	High	Assumed equal to stem	-7[a]	-3.25[b]	-3.5[c]
slope_VC_Leaf	$\%.MPa^{-1}$	Slope of rate of leaf embolism spread at $P50_{Leaf}$	Low	Assumed equal to stem	30[a]	71[b]	135[c]
P12_gs	MPa	Water potential causing 12% stomatal closure	High	Derived from collected TLP	-1.81[d]	-1.7[e]	-1.39[c]
P88_gs	MPa	Water potential causing 88% stomatal closure	High	Derived from collected TLP	-2.69[d]	-2.47[e]	-2.06[c]
epsilonSym_Stem	MPa	Modulus of elasticity of the stem symplast	Intermediate	Collected in literature	8.84[d]	10[e]	10[c]
PiFullTurgor_Stem	MPa	Osmotic potential at full turgor of the stem symplast	Intermediate	Collected in literature	-1.89[d]	-2.08[e]	-1.8[c]
epsilonSym_Leaf	MPa	Modulus of elasticity of the leaf symplast	Intermediate	Assumed equal to stem	8.84[d]	10	10
PiFullTurgor_Leaf	MPa	Osmotic potential at full turgor of the leaf symplast	Intermediate	Assumed equal to stem	-1.89[d]	-2.08	-2.08
LDMC	$mg.g^{-1}$	Leaf dry matter content	/	Collected in literature	500[b]	400[b]	500[b]
LMA	$g.m^{-2}_{leaf}$	Leaf mass per projected leaf area	/	Collected in literature	165[f]	65[f]	106[f]
gmin20	$mmol.m^{-2}_{leaf}.s^{-1}$	Cuticular conductance at 20°C	High	Collected in literature	1.2[d]	2.92[b]	2[c]
gmin_S	$mmol.m^{-2}_{leaf}.s^{-1}$	Stem conductance	High	Assumed equal to gmin20	1.2[d]	2.92[b]	2[c]
LAI_{max}	$m_{leaf}^2.m_{soil}^{-2}$	Maximum leaf area index of the stand	High	Field observation	2.7	4.5	4.2

[a]*Ruffaut et al., 2023;* [b]*Personal data;* [c]*Belen Acuna-Miguez, under review;* [d]*Veuillen et al., 2026;* [e]*Kunert, 2025;* [f]*Diaz et al., 2022.*

**Based on the responses of the simulated time to hydraulic failure to 20% of variation of the parameters, as documented in Ruffault et al. (2022).*

Table S2. *Summary of all species and individual dependent ranges of parameters*

Parameter	Units	*Quercus ilex* L.		*Abies alba* Mill.		*Fagus sylvatica* L.	
Foliage	/	Evergreen		Evergreen		Deciduous	
LAI_{max}	$m_{leaf}^2.m_{soil}^{-2}$	2.7		4.2		4.5	
P_{50}*	MPa	-7[a]		-3.5[c]		-3.25[f]	
Slope*	$\%.MPa^{-1}$	30[a]		135[c]		71[f]	
LDMC	$mg.g^{-1}$	500		500		400	
LMA	$g.m^{-2}_{leaf}$	165[i]		106[i]		65[i]	
F_{crit}	°C	450		450		350	
		Tolerant	Avoidant	Tolerant	Avoidant	Tolerant	Avoidant
g_{min}**	$mmol.m^{-2}_{leaf}.s^{-1}$	1.2[b]		2[c]	1.6[d]	2.92[f]	1.7[g]
epsilonSym*	MPa	16.2[b]	8.84[b]	10[c]		10[h]	
PiFullTurgor*	MPa	-2.81[b]	-1.89[b]	-1.8[c]		-2.08[h]	
P12_gs	MPa	-2.34[b]	-1.81[b]	-1.67[e]	-1.39[c]	-1.67[h]	-1.6[f]
P88_gs	MPa	-3.47[b]	-2.69[b]	-2.47[e]	-2.06[c]	-2.47[h]	-2.38[f]

** For stem and leaf values. ** For cuticular and stem conductance.*

[a] Ruffaut et al., 2023; [b] Veuillen et al., 2026; [c] Belen Acuna-Miguez, under review; [d] Copie et al., 2025; [e] Kunert & Tomaskova, 2020; [f]Personal data; [g] Waite et al., 2024; [h] Kunert, 2025; [i] Diaz et al. 2022

Table S3. *Description, source and values of the site-specific soil parameters implemented*

Parameter	Unit	Description	Source of the value	Implemented values		
				Layer	Rustrel	Mont-Ventoux
$Depth_j$	m	Maximum depth of soil layer *j*	Own observation and assumptions	*j* = 1	0.2	0.3
				j = 2	0.6	0.7
				j = 3	4	4
RFC_j	%	Rock fragment content in soil layer *j*	Own observation then adjustment	*j* = 1	28	54
				j = 2	65	66
				j = 3	75	86
K_{sat}	$mmol.m^{-2}.s^{-1}.MPa^{-1}$	Soil hydraulic conductivity at saturation	From Carsel and Parrish (1988)		1.1	1.5
Saturation capacity	$cm^3.cm^{-3}$	Soil water content at saturation	From Carsel and Parrish (1988)		0.36	0.46
Residual capacity	$cm^3.cm^{-3}$	Residual soil water content	From Carsel and Parrish (1988)		0.07	0.034
n_vg	/	Van Genuchten - Mualem pore size distribution index	From Ghanbarian-Alavijeh et al. (2010)		1.23	1.37

Table S4. *Summary of all soil parameter*

Parameter	Unit	Description	Implemented values	
			Rustrel	Mont-Ventoux
$Depth_j$	m	Maximum depth of soil layer *j*	0.2 .6 4	0.3 0.7 4
RFC_j	m	Rock fragment content in soil layer *j*	28 65 75	54 66 86
K_{sat}	$mmol.m^{-2}.s^{-1}.MPa^{-1}$	Soil hydraulic conductivity at saturation	1.1	1.5
Saturation capacity	$cm^3.cm^{-3}$	Soil water content at saturation	0.36	0.46
Residual capacity	$cm^3.cm^{-3}$	Residual soil water content	0.07	0.034
n_vg	/	Van Genuchten - Mualem pore size distribution index	1.23	1.37
alpha_VG	MPa^{-1}	Van Genuchten - Mualem shape parameter	0.005	
I_vg	/	Van Genuchten - Mualem tortuasity	0.5	
gsoil	$mmol.m^{-2}.s^{-1}$	Soil conductance to vapour	30	
PsoilAtFieldCapacity	MPa	Soil water potential at field capacity	0.0033	

Figure S1 *Evolution of RMSE of computed with Holm oak predawn leaf water potential according to the* TAW_{Deep}

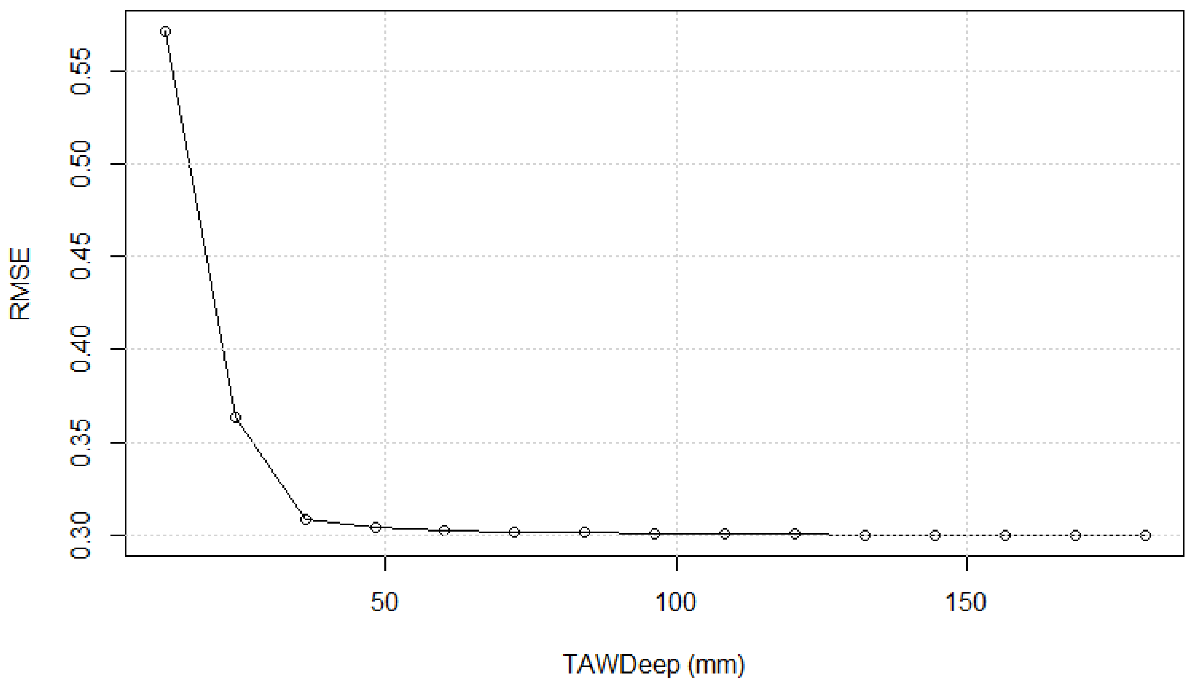

Figure S2. *Evolution of RMSE of computed with Fir predawn leaf water potential according to the* TAW_{Deep}

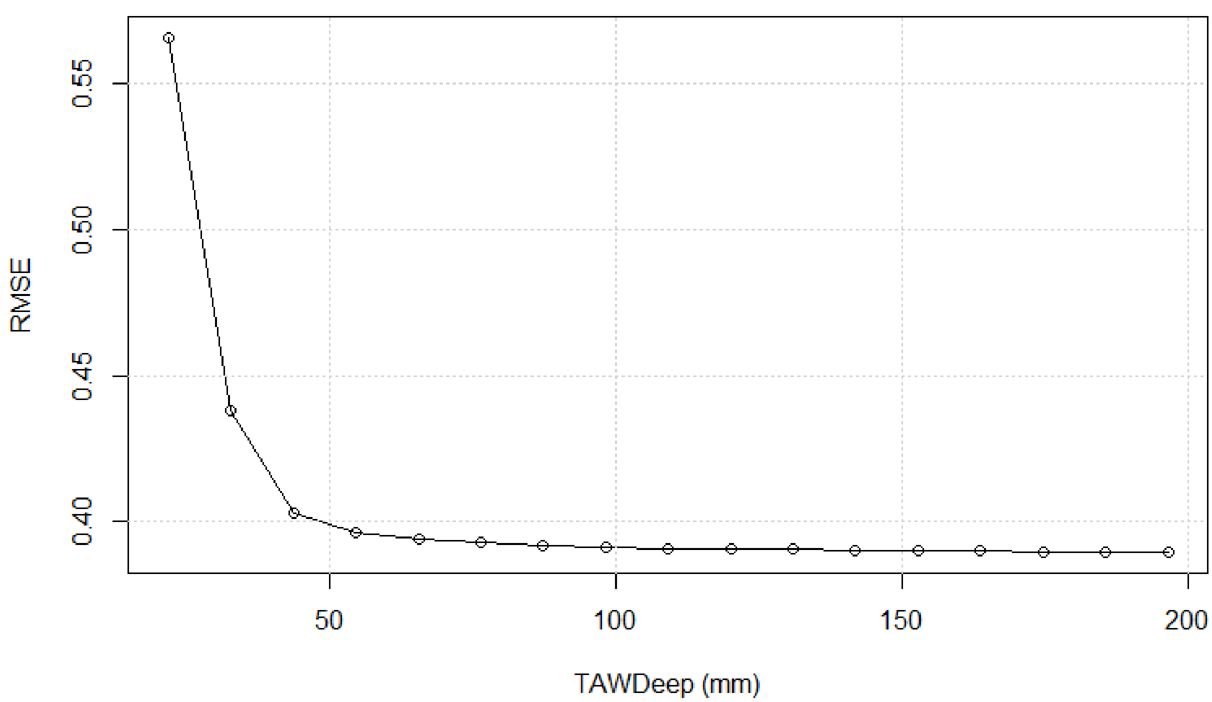

Figure S3. *Evolution of RMSE of computed with Beeches predawn leaf water potential according to the TAW$_{Deep}$*

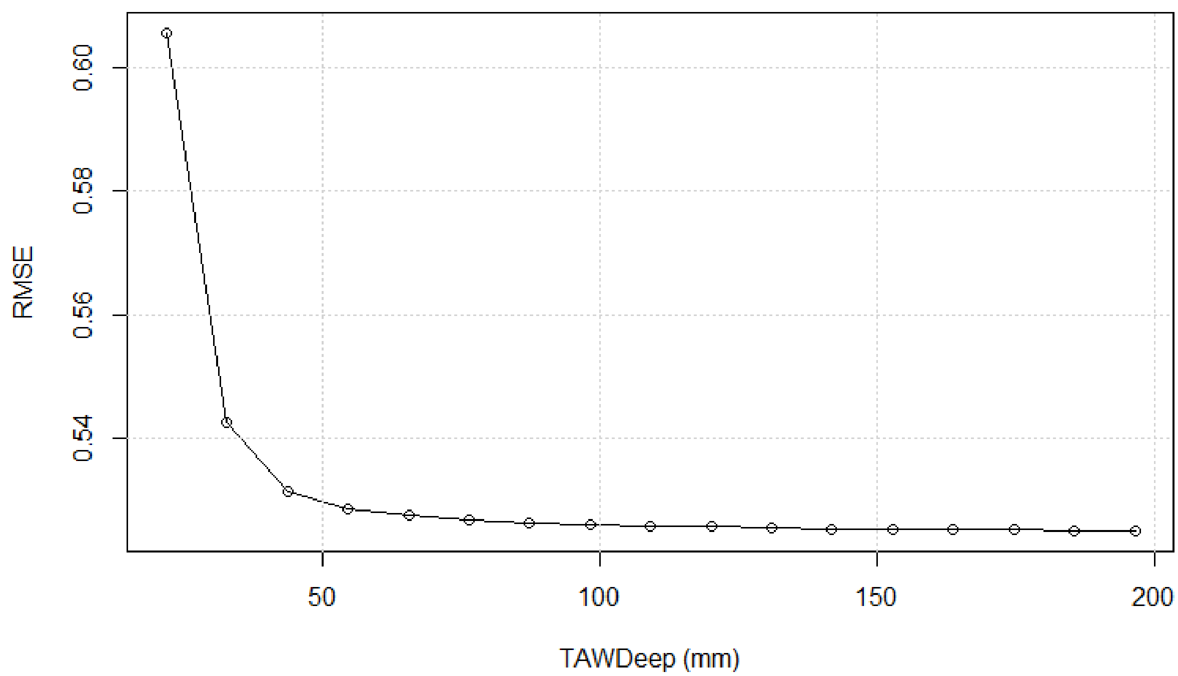

Figure S4 *Results of the calibrated model simulations for the beech trees of Mont-Ventoux (Fig.* ***2****). a. Time series of deep reservoir use relative to evapotranspired volumes (f_{DW}); b. Time series of predawn water potential (Ψp); c. and d. Correlation between observed and simulated values.*

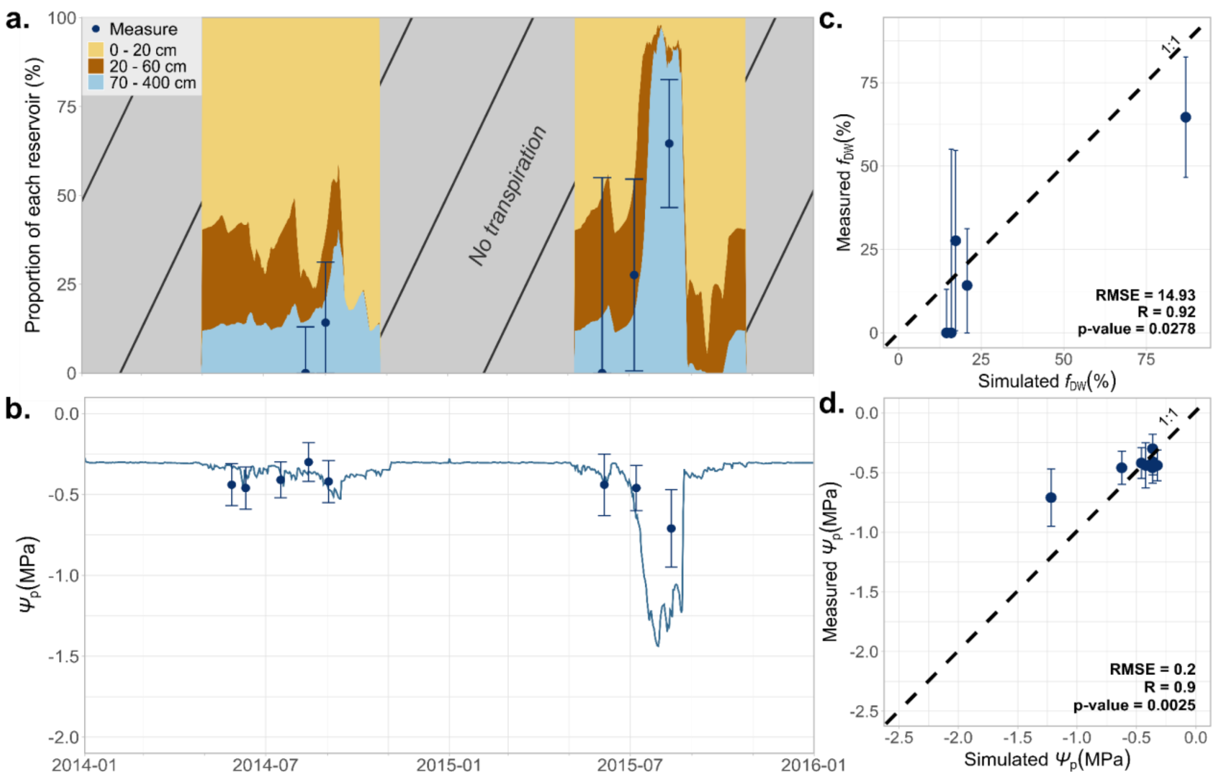

Figure S5 *Results of the calibrated model simulations for the Silver firs of Mont-Ventoux (Fig.* ***2****). a. Time series of deep reservoir use relative to evapotranspired volumes (f_{DW}); b. Time series of predawn water potential (Ψp); c. and d. Correlation between observed and simulated values.*

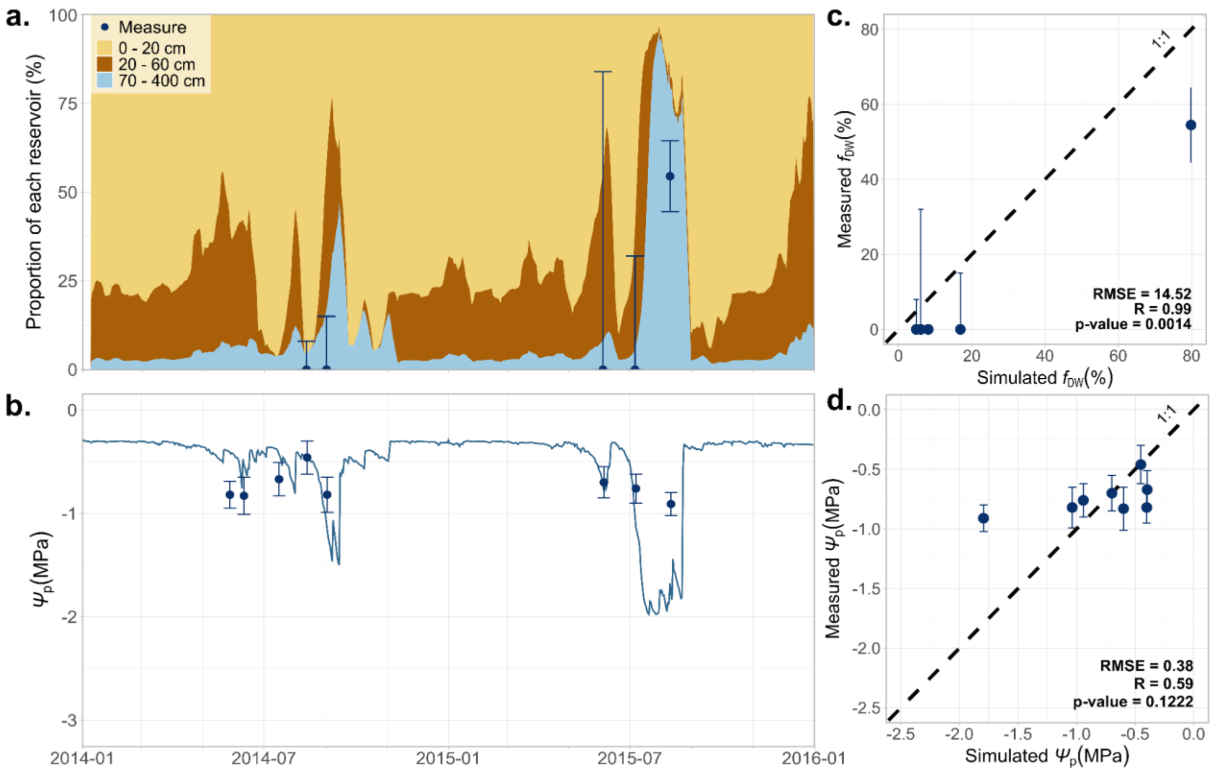

Figure S6 *Rainfall (a.), proportion of each reservoir the water transpired by oak (b.), base water potential* (Ψp) *(c.).*

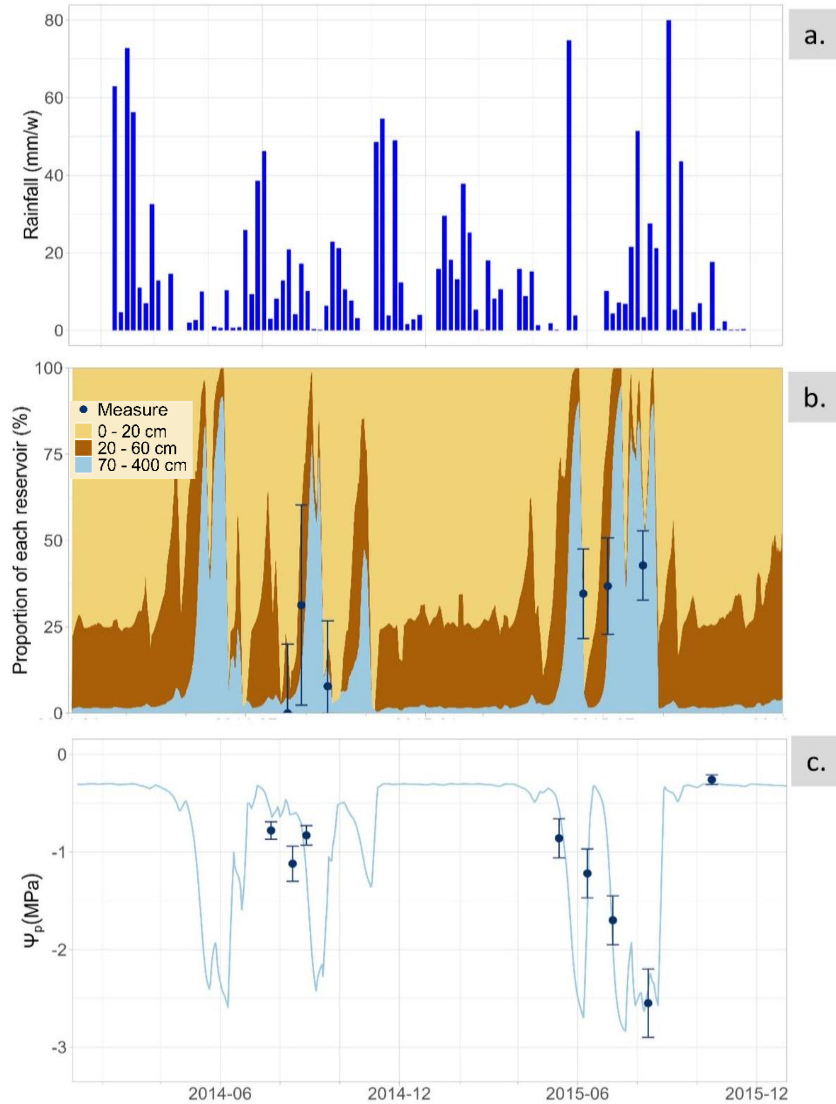

Figure S7 *Rainfall (a.), proportion of each reservoir the water transpired by beech (b.), base water potential* (Ψp) *(c.).*

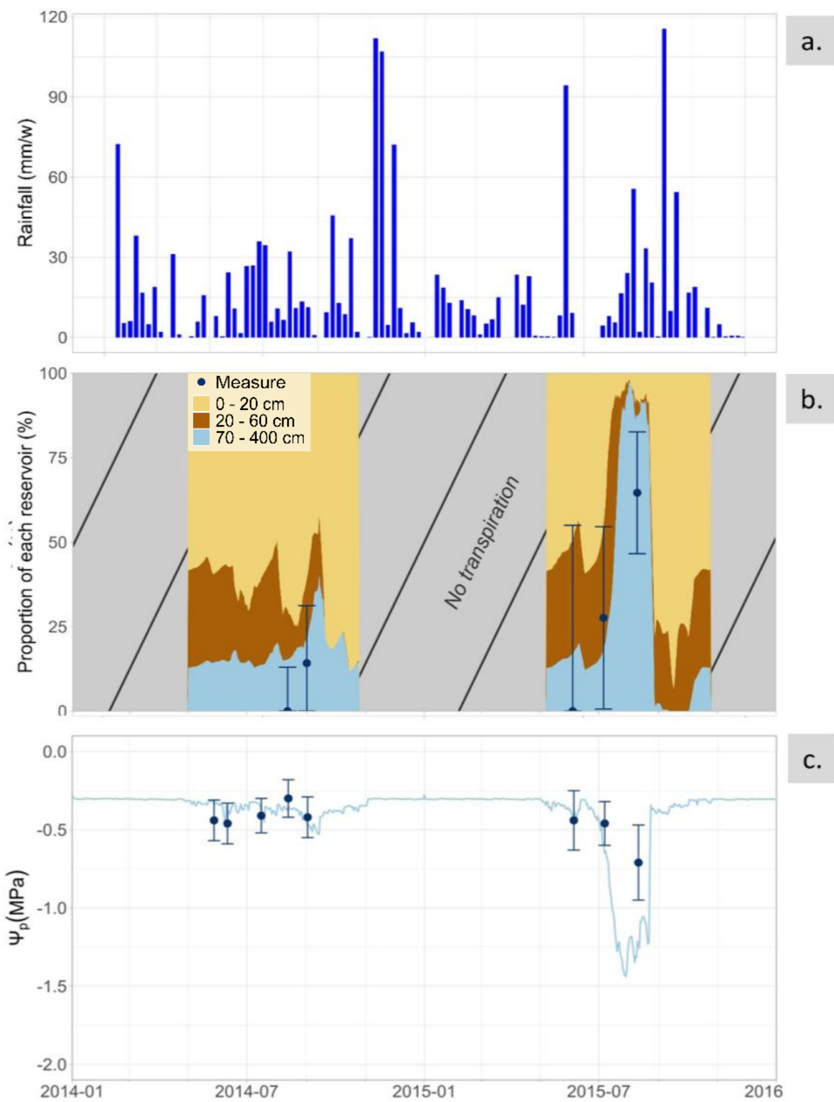

Figure S8 *Rainfall (a.), proportion of each reservoir the water transpired by firs (b.), base water potential* (Ψp) *(c.).*

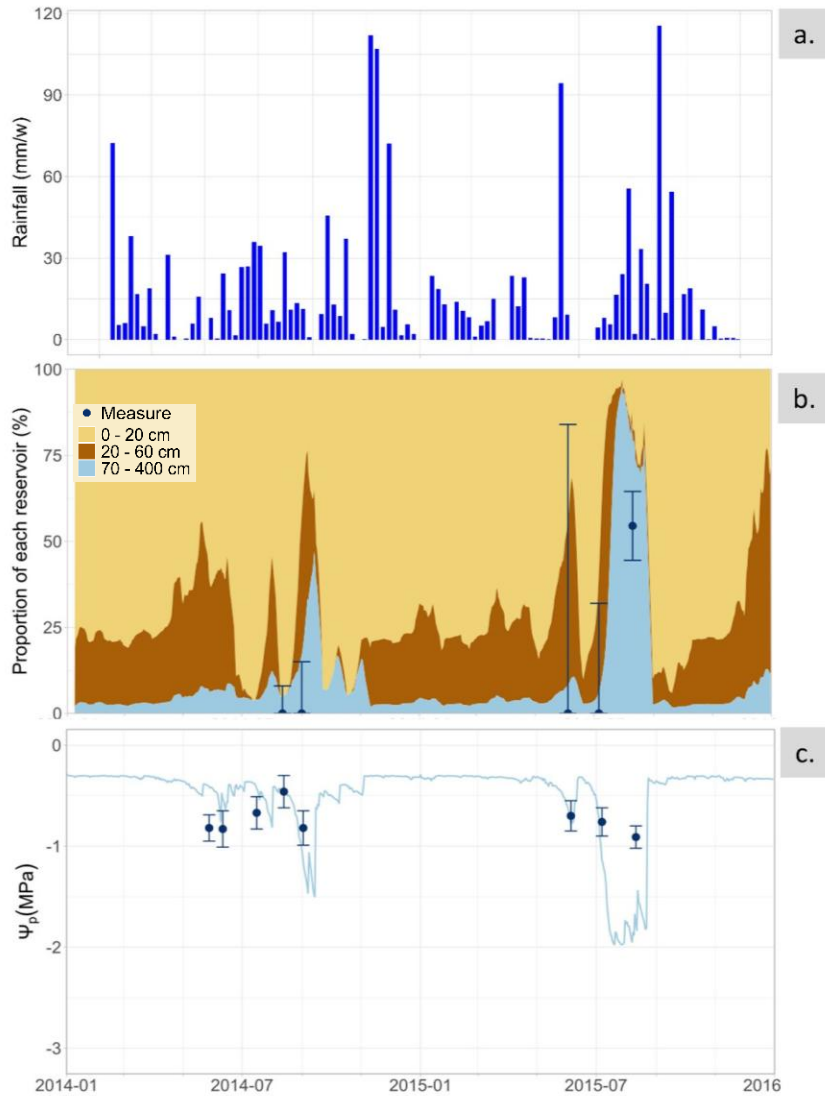

Figure S9. *Dynamics of Relative Water Content (REW), stomatal conductance (g_s), Percentage Loss of Conductivity (PLC) and base potentials (Ψp) of a Holm oak during a theoretical continuous drought, with different proportions of the root system in the deep layer (f_{DR}) and TAW_{Deep} = 65 mm. The dashed line corresponds to the oak TLP and the time it is reached.*

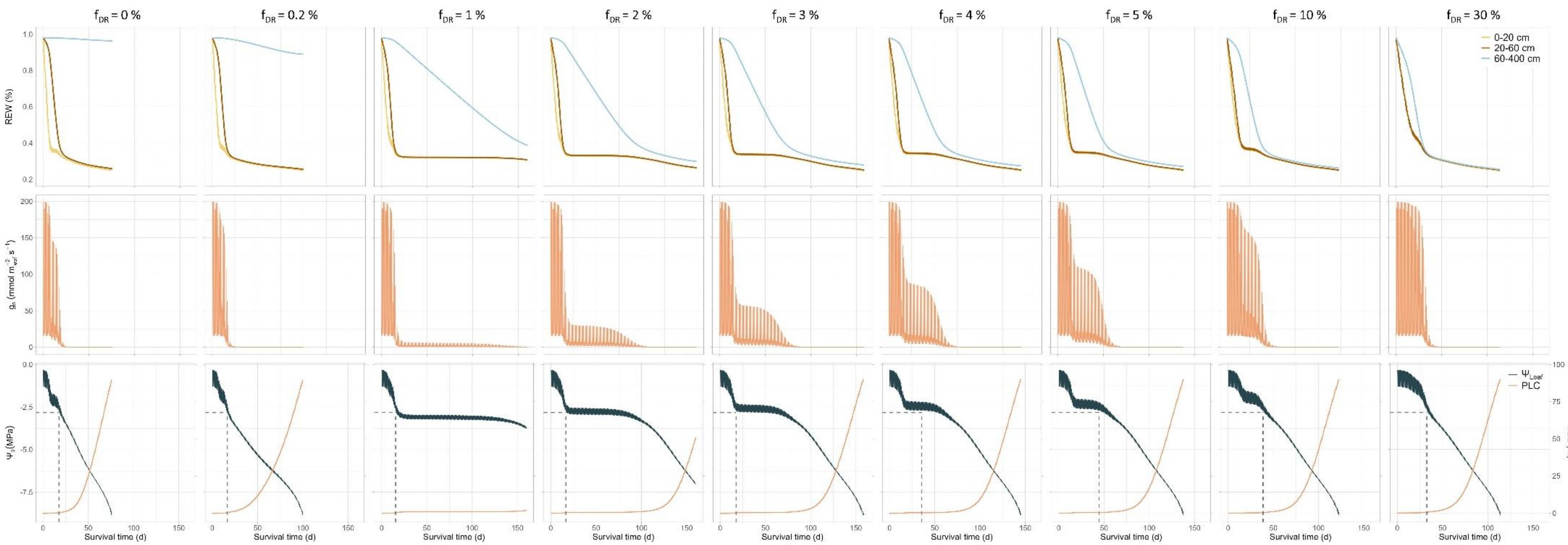

Bibliography

Copie, A., Scotti-Saintagne, C., Lefèvre, F., Cochard, H., Delzon, S., Dumas, P.-J., Gounelle, D., Herbette, S., Jean, F., Mariotte, N., Mencuccini, M., Scotti, I., Martin-StPaul, N., 2025. Beyond Proxies: Towards ecophysiological indicators of drought resistance for forest management. Tree Physiology 45, 9. https://doi.org/10.1093/treephys/tpaf090

Díaz, S., Kattge, J., Cornelissen, J.H.C., Wright, I.J., Lavorel, S., Dray, S., Reu, B., Kleyer, M., Wirth, C., Prentice, I.C., Garnier, E., Bönisch, G., Westoby, M., Poorter, H., Reich, P.B., Moles, A.T., Dickie, J., Zanne, A.E., Chave, J., Wright, S.J., Sheremetiev, S.N., Jactel, H., Baraloto, C., Cerabolini, B.E.L., Pierce, S., Shipley, B., Casanoves, F., Joswig, J.S., Günther, A., Falczuk, V., Rüger, N., Mahecha, M.D., Gorné, L.D., Amiaud, B., Atkin, O.K., Bahn, M., Baldocchi, et al., 2022. The global spectrum of plant form and function: enhanced species-level trait dataset. Sci Data 9, 755. https://doi.org/10.1038/s41597-022-01774-9

Kunert, N., 2025. Rapid springtime leaf osmotic adjustment, but low late-seasonal and interannual variation in leaf turgor loss points in three temperate tree species. J. For. Res. 36, 46. https://doi.org/10.1007/s11676-025-01846-7

Kunert, N., Tomaskova, I., 2020. Leaf turgor loss point at full hydration for 41 native and introduced tree and shrub species from Central Europe. Journal of Plant Ecology 13, 754–756. https://doi.org/10.1093/jpe/rtaa059

Ruffault, J., Limousin, J., Pimont, F., Dupuy, J., De Càceres, M., Cochard, H., Mouillot, F., Blackman, C.J., Torres-Ruiz, J.M., Parsons, R.A., Moreno, M., Delzon, S., Jansen, S., Olioso, A., Choat, B., Martin-StPaul, N., 2023. Plant hydraulic modelling of leaf and canopy fuel moisture content reveals increasing vulnerability of a Mediterranean forest to wildfires under extreme drought. New Phytologist 237, 1256–1269. https://doi.org/10.1111/nph.18614

Veuillen, L., Simioni, G., De Cáceres, M., Badel, E., Carrière, S.D., Cochard, H., Courbet, F., Doussan, C., Druel, A., Ladier, J., Prévosto, B., Raynal, K., Martin-StPaul, N., 2026. Thinning enhances hydraulic safety but not growth resistance to drought in Atlas cedar on the long-term. Agricultural and Forest Meteorology 378, 111019. https://doi.org/10.1016/j.agrformet.2026.111019

Waite, P.-A., Riedel, V.P., Link, R.M., Beldman, I., Kumar, M., Nain, P., Panagoulias, M., Schuldt, B., 2026. Coordinated hydraulic traits predict the time to critical hydraulic failure in temperate broad-leaved and conifer tree species. Plant Physiol 201, kiag177. https://doi.org/10.1093/plphys/kiag177